Journal of Coastal Research	SI	59	49-60	West Palm Beach, Florida	2011

Modeling Regional-Scale Sediment Transport and Medium-Term Morphology Change at a Dual-Inlet System Examined with the Coastal Modeling System (CMS): A Case Study at Johns Pass and Blind Pass, West-Central Florida

www.cerf-jcr.org

Ping Wang[†], Tanya M. Beck[‡], and Tiffany M. Roberts[†]

[†]Department of Geology
University of South Florida
Tampa, FL, 33620 USA

[‡]U.S. Army Engineer Research and Development Center,
Coastal and Hydraulics Laboratory
Vicksburg, MS, 39180, USA

ABSTRACT

WANG, P.; BECK, T.M., and ROBERTS, T.M., 2011. Modeling Regional-Scale Sediment Transport and Medium-Term Morphology Change at a Dual-Inlet System Examined with the Coastal Modeling System (CMS): A Case Study at Johns Pass and Blind Pass, West-Central Florida. *In:* Roberts, T.M., Rosati, J.D., and Wang, P. (eds.), *Proceedings, Symposium to Honor Dr. Nicholas C. Kraus,* Journal of Coastal Research, Special Issue, No. 59, pp. 49-60. West Palm Beach (Florida), ISSN 0749-0208.

The Coastal Modeling System (CMS), developed by the US Army Engineer Research and Development Center's (ERDC) Coastal Inlets Research Program (CIRP), is applied to model morphology change at a dual-inlet system, the Johns Pass and Blind Pass system in West-Central Florida. The CMS combines computation of current, wave, and sediment transport, leading to the prediction of morphology change at tidal inlets and the surrounding beaches. Medium-term CMS runs, with simulated times of 1.2 to 1.6 years, were completed and compared with extensive field data. Stronger tidal flow through the dominating Johns Pass and weaker flow through the secondary Blind Pass were calculated, indicating that the model reproduced an essential aspect of this interactive two-inlet system. The complicated wave refraction and breaking over the ebb tidal deltas and along the adjacent shorelines were accurately modeled, leading to a realistic representation of the wave-current interaction. Wave-breaking induced elevated sediment suspension and transport were described by the model. The predicted morphology change agreed well with field data. The CMS captured several key spatial trends of morphology change, *e.g.*, erosion along the downdrift beach and accretion at the attachment point. The computed 32,000 m^3/yr sedimentation volume in the dredge pit at the updrift side of Blind Pass matched the measured value of 35,000 m^3/yr with a similar spatial distribution pattern, suggesting that the calculated net longshore sediment transport rates are accurate. The computed sedimentation rate of 60,000 m^3/yr at a designed dredge pit on Johns Pass ebb-delta agrees with the generally accepted gross longshore transport rate. Rapid and large morphology change in response to high wave-energy events is predicted and is consistent with field observations.

ADDITIONAL INDEX WORDS: *Nearshore sediment transport, coastal morphology, numerical modeling, dredging, tidal inlets, ebb tidal delta, channel infilling, tides, waves, Florida.*

INTRODUCTION

Tidal inlets provide a link between the coastal ocean and back-barrier bay, exchanging water, sediment, nutrients, and other materials between them. Sediment transport in the vicinity of tidal inlets is active and complicated, driven by simultaneously acting hydrodynamic forcing including tidal currents, breaking and non-breaking waves, wave-driven currents, and wind-driven currents. The complicated interaction of these hydrodynamic processes plays a significant role in controlling the rate and patterns of sediment transport. As a consequence, the morphologic features associated with tidal inlets and the adjacent beaches are highly variable, ranging from deep channels to shallow shoals and with a variety of bed forms across the ebb and flood tidal deltas. Many inlets also support maintained navigation channels, further complicating the natural system by introducing anthropogenic controls (Kraus, 2009). Dean (1988) concluded that more than 80% of the erosion along the Florida coast can be directly linked to tidal inlets. Rapid and large morphology changes are typically measured at tidal inlets and their adjacent beaches, making them one of the most dynamic systems in the nearshore environment. Therefore, mathematical modeling of sediment transport and morphology change in the vicinity of tidal inlets is a challenging task.

Many bays along the microtidal, mixed energy West-Central Florida coast are served by more than one tidal inlet, and the Gulf Intracoastal Waterway (GIWW) may intersect the bay channel. If the multiple inlets are relatively close to each other, the morphology change at one inlet can be directly influenced by

DOI: 10.2112/SI59-006.1 received 12 November 2009; accepted 15 June 2010.

the evolution of the other inlets (Aubrey and Giese, 1993; van de Kreeke, 1990; Fitzgerald, 1996; van de Kreeke *et al.*, 2008). The Johns Pass and Blind Pass system is an excellent example of morphology evolution due to the interaction of the two inlets in relative close proximity. Modeling the processes at a multiple inlet system presents an additional challenge to an already complicated process.

In this study, medium-term (defined here as 1 to 2 years) morphology change at Johns Pass and Blind Pass are examined through analysis of field measurements and numerical modeling. The state-of-the-art numerical model, Coastal Modeling System (CMS), is employed for the numerical modeling analysis. The CMS was developed by the US Army Engineer Research and Development Center's (ERDC) Coastal Inlets Research Program (CIRP). The CMS was developed specifically for integrated numerical modeling of hydrodynamics (Buttolph *et al.*, 2006; Reed *et al.*, this issue; Wu *et al.*, this issue; Lin *et al.*, this issue), sediment transport (Larson and Camenen, this issue), and morphology changes (Sanchez and Wu, this issue) associated with tidal inlets. The overall goal of this study is to examine the capability of the CMS in calculating sediment transport and morphology change at the Johns Pass-Blind Pass dual-inlet system. Extensive bathymetric and hydrodynamic data were collected at these two inlets, providing a large dataset for evaluating and verifying the calculations. Specifically, the objective of this study is to apply the CMS over a period of 1 to 2 years to examine 1) regional flow patterns at the dual-inlet system; 2) wave propagation over the complicated bathymetry; 3) wave-current interaction at the tidal inlets; 4) regional patterns of sediment transport; and 5) medium-term morphology change. The numerical calculations are compared, both quantitatively and qualitatively, with the extensive field dataset.

STUDY AREA

Johns Pass and Blind Pass, separated by the 6-km long Treasure Island, service a portion of Boca Ciega Bay along the West-Central Florida coast (Figure 1). Regionally, the Johns Pass-Blind Pass system is the part of the West-Central Florida barrier-island chain that extends north from the mouth of Tampa Bay. The entire area, from the beaches to the inlets to the back-bay, is densely developed. Several causeways and bridges and numerous dredge and fill finger channels dissect the back-barrier bay, especially within the water body landward of Blind Pass.

The overall wave energy along this coast is mild with average breaker heights for West-Central Florida estimated to be 25-30 cm (Tanner, 1960). Generally, wave-induced sediment transport in the study area tends to be episodic, controlled by high-energy events typically associated with winter cold front passages (Elko *et al.*, 2005; Elko and Wang, 2007). The wind and waves during these events tend to come from a northerly direction, driving a southward longshore sediment transport. The study area is characteristic of a mixed tidal regime. The spring tide is diurnal with a range of roughly 0.8 to 1.2 m, and the neap tide is semi-diurnal with a range of 0.4 to 0.5 m. Siliciclastic sediment along the West-Central Florida coast is primarily composed of fine quartz sand with a mean grain size of 0.17 mm. Mean grain size variation in the study area is relatively small, ranging from 0.2 mm to 0.5 mm, with the varying concentrations of shell debris

Figure 1. The Johns Pass and Blind Pass inlet system, illustrated with a 2004 aerial photograph.

contributing to the coarser grains. The largest grain sizes are found in the channel thalweg where coarse lag deposits are concentrated.

Johns Pass is a stabilized inlet located between Treasure Island to the south and Sand Key to the north. Since its opening in 1848 by a hurricane, Johns Pass has gradually become the dominant inlet of the Johns Pass-Blind Pass system, capturing 70 - 80% of the tidal prism (Mehta *et al.*, 1976; CPE, 1993). As shown in Figure 1, the portion of Boca Ciega Bay, directly landward of Johns Pass, is larger and not as dissected by man-made islands as compared to the portion landward of Blind Pass. John Pass is characteristic of a mixed-energy inlet with a large ebb-tidal delta, skewed to the south in the direction of the southward net longshore sediment transport (Figure 2). The downdrift attachment is apparent as illustrated by the protruding shoreline (Figure 3). Sunshine Beach, updrift (north) of the attachment point, experiences chronic erosion, whereas, the beach downdrift (south) of the attachment point is wide, with up to 300 m of dry beach, and has demonstrated an accretionary trend over the last two decades. Johns Pass and its ebb-tidal delta have been dredged in 1960, 1961, 1966, 1971, 1980-1985, 1988, 1991, and 2000 (Barnard, 1998). The dredged sand is typically used to nourish the adjacent beaches.

The origin of Blind Pass is not historically recorded (within the last two centuries). Blind Pass appeared to have been the dominant inlet serving Boca Ciega Bay, with large flood- and ebb-tidal deltas, before the opening of Johns Pass in 1848. As Johns Pass gradually captured a substantial portion of the tidal prism, the net longshore sediment transport caused rapid southward migration of Blind Pass (Figure 1). Blind Pass was eventually stabilized with jetties beginning in 1937, modifying the entrance channel into a sharp 90-deg turn with a wide (160 m) entrance basin (CPE, 1992). Between the 1940s and 1960s, extensive dredge-and-fill construction was conducted in Boca Ciega Bay (Figure 1). The engineered islands, as well as the construction of several causeways, resulted in significant reduction of back-bay area and thus a continued decrease in tidal

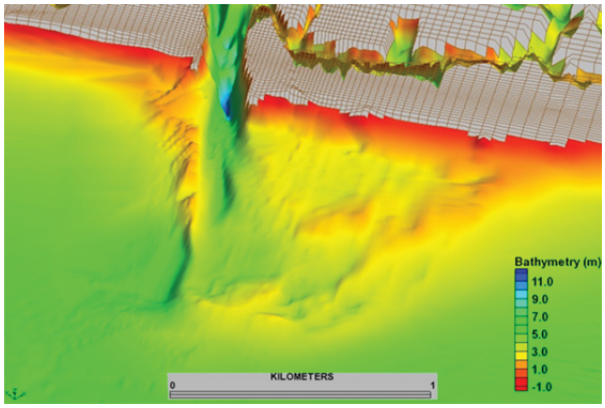

Figure 2. The Johns Pass ebb-tidal delta surveyed in 2008. The depth (positive number) is relative to mean sea level. The delta is skewed to the south, controlled by the southward longshore sediment transport. Note the complicated bathymetry with numerous bars.

Figure 3. The attachment point of Johns Pass ebb-tidal delta. Note the wide beach at and south of the attachment and narrow beach north. The aerial photo is taken in 2007.

prism. The wide entrance channel, relative to the small tidal prism, at Blind Pass has become an effective trap for the southward longshore transport allowing little to no bypassing to downdrift beaches. Dredging operations were conducted in 1937, 1964, 1969, 1975, 1979, 1983, 1990, and 2000 to maintain the entrance channel at Blind Pass. The dredged sand was used to nourish adjacent beaches, especially the chronically eroding downdrift Upham Beach.

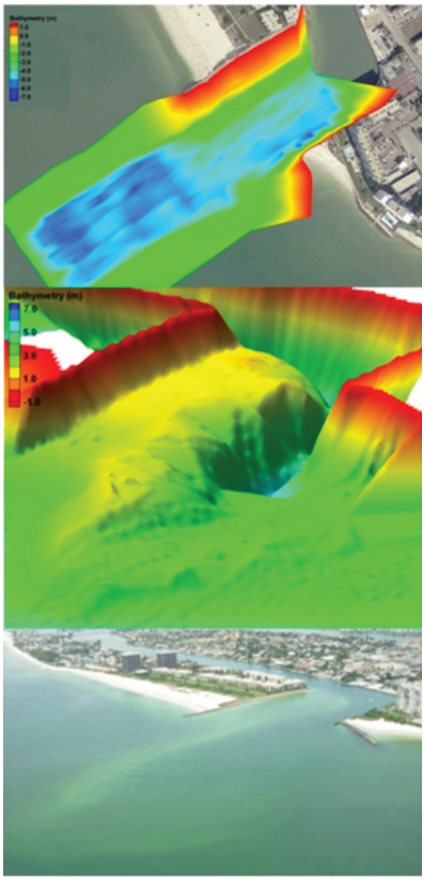

Figure 4. Ebb-tidal delta development at Blind Pass after the dredging in 2000. Top: bathymetry (positive relative to mean sea level) immediately after the dredging; Middle: bathymetry in 2008; Bottom: oblique aerial photo of the ebb-tidal delta taken in July 2008.

A field study aimed at quantifying sedimentation in the channel was conducted after the dredging in the summer of 2000 (Wang *et al.*, 2007). Three years after the dredging operation in 2000, the northern side of the inlet had infilled to a level less than 1 m below mean sea level from the cut depth of approximately 5 m. A considerable amount of sand was transported around the 90-deg turn in the channel and deposited along the landward side of Treasure Island, as indicated by the accreting beach there. The exact amount of sand deposited is not clear. Recently, an ebb-tidal delta, consisting primarily of an updrift channel margin linear bar, has developed with a west-southwest trending orientation (Figure 4). By 2008, eight years after the last dredging, the ebb-tidal delta has become relatively substantial in size with visible wave shoaling and breaking along much of the linear bar during both fair and stormy weathers. The development of the ebb-tidal delta was likely accelerated by the sand introduced to the nearshore system by the recent beach nourishments in 2004 and 2006 on Treasure Island and Long Key (Wang *et al.*, 2008) both north and south of the inlet.

Based on time-series survey data, Wang *et al.* (2007) found that the shoaling rate in the entrance channel of Blind Pass was 35,000 m^3/year during the first two years and reduced to 26,000 m^3 in the third year, likely due to the transport around the corner into the back channels. The inlet largely serves as a total trap for southward longshore sediment transport. Most of the sediment shoaling occurs along the north side of the inlet, corresponding to 1) its proximity to the sand source, 2) limited impoundment at the north jetty, 3) weak ebb flushing due to preferential location of the ebb jet along the south side, and 4) relatively stronger flood current in comparison to ebbing current along the north side. Wave breaking over the shallow north shoal, starting roughly two years following the dredging, also contributes to the sand redistribution further landward into the inlet. Accumulation and erosion patterns in the Blind Pass channel demonstrate a distinct seasonal trend, with typically active sedimentation in the winter driven by frequent cold front passages and sediment redistribution during the calmer summer season (Wang *et al.,* 2007).

The morphodynamics of the adjacent beaches are well understood based on field observations. The beach north and updrift of Johns Pass has been relatively stable over the last decade. Sunshine Beach, south and downdrift of Johns Pass, has shown an erosive trend over the years driven by a reversal of the regional southward longshore transport induced by the wave refraction over the Johns Pass ebb-tidal delta. The beach at and south of the Johns Pass attachment point is accretionary, benefiting from the sand bypassed around the ebb-tidal delta. Sunset Beach, located along the southern portion of Treasure Island, illustrates a chronic erosional trend. Sunset Beach is also located landward of a relict, nearshore dredged pit excavated in the late 1960s for beach nourishment. Both Sunshine Beach and Sunset Beach have been nourished frequently with sand dredged from Johns Pass and Blind Pass, as well as from offshore sources. Upham Beach directly south and downdrift of Blind Pass is a well-documented erosional hot spot driven by a persistent deficit from the net southward longshore transport (Elko *et al.*, 2005; Elko and Wang, 2007). The main causes of erosion at Upham Beach are its proximal location to Blind Pass, which impounds nearly the entire southward longshore sand transport during a typical dredging interval (4-7 years). The beach south of the eroding Upham Beach tends to be accretionary, as the erosional hotspot serves as a feeder beach supplying sand to the downdrift coast (Elko and Wang, 2007).

The CMS is applied here to examine the medium-term morphology changes at the Johns Pass and Blind Pass system. The success of the modeling is examined based on the observed morphology trends as discussed above. This study focuses on the analyses and interpretation of the calculated regional-scale sediment transport and morphology change. General hydrodynamics modeling of waves and currents are discussed in other papers (Lin *et al.*, this issue; Sanchez and Wu, this issue) in this volume.

METHODOLOGY

Coastal Modeling System (CMS)

The Coastal Modeling System (CMS) was developed by the US Army Engineer Research and Development Center's (ERDC) Coastal Inlets Research Program (CIRP: http://cirp.wes.army.mil). The CMS is a process-based suite of models that integrate hydrodynamics, sediment transport, and morphology change through the coupling of two modules, CMS-Flow and CMS-Wave. CMS-Flow solves depth-integrated continuity and momentum equations using a finite-volume method (Kraus and Militello, 1999; Buttolph, *et al.*, 2006; Reed *et al.*, this issue). The hydrodynamics in the Johns Pass-Blind Pass model are driven by tidal forcing measured at the ocean boundary; however, wind, flow, and other water surface elevation forcing can also be applied. The unified sediment transport formula, the Lund-CIRP (Camenen and Larson, 2007; Larson and Camenen, this issue), and a non-equilibrium transport formula (NET) (Wu, 2007; Sanchez and Wu, this issue) are applied for the computation of sediment transport and morphology change. The sediment transport computation includes transport of non-cohesive sediments by both current and wave (non-breaking and breaking waves). Non-equilibrium transport, as represented in the CMS for morphology computation, includes advection and diffusion of the entrained sediments. Given the large areas of shallow water typically associated with tidal inlets, *e.g.* over the ebb tidal delta and near the shoreline, accurate representation of wave breaking and elevated sediment suspension and transport induced by breaking waves is essential. Compared to a typical temporal scale of hydrodynamics (*e.g.*, waves and tides), morphology changes occur over a longer period. Time efficient computation and robust numerical stability are vital to morphology modeling (Wu *et al.*, this issue).

The CMS-flow (Reed *et al.*, this issue) is coupled with the CMS-Wave (Lin *et al.*, this issue), a steady-state, half-plane, spectral transformation wave model using a finite-difference, forward-marching implicit scheme. CMS-Wave is an improved and modified version of the wave model WABED for inlet applications (Mase and Kitano 2000; Mase, 2001; Mase *et al.*, 2005; Lin *et al.*, 2006; Lin *et al.*, 2008). Wave refraction, shoaling, reflection, diffraction, and breaking are computed, as well as the influence of wind. The input wave conditions to CMS-Wave can be measured directional wave spectra, or the spectrum can be generated based on statistical wave parameters including wave height, wave period, incident wave angle, spectral peakedness, and directional spreading. Several types of spectra can be generated, including the TMA, JONSWAP, Bretschneider (ITTC), Pierson-Moskowitz, and Ochi-Hubble Double Peak Spectrum (Lin *et al.*, 2008). Recently, wave setup and runup have been added (Lin *et al.*, this issue). The breaking induced radiation stress is computed and passed to CMS-Flow for the calculation of the wave-induced longshore current, in addition to wave height, period, and setup, all of which are necessary for calculating sediment transport under combined waves and current.

Model Setup

An accurate bathymetric grid is essential for representative modeling because wave propagation is strongly influenced by nearshore bathymetry. In addition, high spatial resolution is

necessary for adequately resolving the inlets. The nearshore, the two inlets, and the back-barrier bay were surveyed between 2006 and 2008. The bathymetry surveys were conducted using a synchronized, precision echo sounder and RTK-GPS (Real Time Kinematic Global Positioning System). Beach and nearshore surveys were conducted using an electronic total survey station following standard level-transit survey procedures. Dense survey lines were run over the inlet channels and ebb-tidal deltas to ensure an accurate measure of the complicated bathymetry. The numerous finger channels in the back-bay were mapped by dense survey transects including those along the seawall. Recent beach profiles were consulted to ensure accurate delineation of shoreline position and nearshore bathymetry, which has significant control on wave breaking and therefore nearshore sediment transport. Aerial photographs were overlain on the bathymetry to better define sharp boundaries, particularly those of structures and seawalls. Data from the NOAA NGDC Coastal Relief Model (http://ngdc.noaa.gov) covered the offshore regions not surveyed by this study.

The CMS grid is constructed based on the above bathymetric data (Figure 5). A variable sized rectangular-cell grid system, with a spatial resolution ranging from 10x10 m in the vicinity of the channels, the ebb-tidal deltas, and the nearshore zone to 80x100 m near the ocean boundary, was generated with the main axes (oriented along 35 deg – 215 deg) parallel to the regional shoreline and bathymetry trend. The great depth variations associated with deep channels, and shallow flood- and ebb-tidal deltas are apparent. The Johns Pass and Blind Pass channels each had at least 16 cells to ensure accurate representation of the velocity distribution across the inlet channel. High resolution is also needed to predict patterns of sediment transport, and deposition and erosion (Wang *et al.*, 2007). Small grid cells were specified in the nearshore zone and over the shallow portion of the ebb-tidal deltas to capture wave breaking and breaking-induced sediment transport.

Another important aspect of the grid-system setup involves the determination of boundaries. Because the relevant portion of the Boca Ciega Bay does not have any significant river input, the landward boundary around the bay is easily defined. The seaward boundary should extend well beyond the distal edge of the influence of the ebb jet and should be deep enough that significant shoaling does not occur at the boundary under energetic wave conditions. However, the seaward boundary should be set at an offshore location that allows for a reasonable model computation time, which is proportional to the number of cells. The goal of this study was to calculate medium-term (1 to 2 years) morphology change, within a reasonable computation time frame, *e.g.*, less than 2 to 3 weeks with the available explicit-solution version of the CMS at the time this study was done; therefore, the seaward boundary for this study was set at roughly 3 km offshore the inlets at a water depth roughly equal or greater than 7 m. This boundary is much deeper than the active DOC (Wang and Davis, 1999). The north boundary is set where the bay merges into a narrow channel (GIWW).

The south boundary of the Johns Pass and Blind Pass system connects to the southern Boca Ciega Bay and eventually links to Tampa Bay (Figure 1). There is no physical separation between the northern and southern Boca Ciega Bay. It was not considered practical or necessary to include all the connected

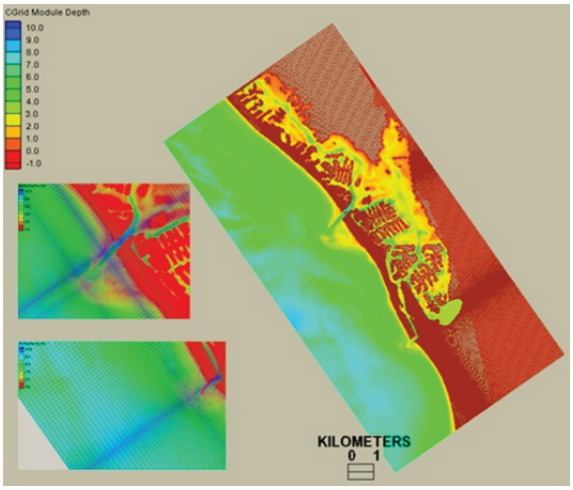

Figure 5. The model domain of the Johns Pass and Blind Pass system. The depth (positive) is relative to mean sea level. The insert illustrate the refined dense grid in the inlet channels and over the ebb deltas.

water bodies for medium-term morphology model runs as this would increases computation time and it becomes difficult to define a boundary limit in the vicinity of the greater Tampa Bay Estuary. To better define this watershed boundary, the following tidal prism method was performed. Tidal prism can be calculated using several methods (Bruun, 1978). Based on a discharge approach, the tidal prism through Johns Pass and Blind Pass was calculated by multiplying the measured tidal current speed by the cross-section at each inlet, while from a storage approach, the tidal prism can be obtained via multiplying the tidal range by the bay area. Both methods should yield identical values of tidal prism. Because the effective bay area is not known in this case, by equating the two methods, the bay area and therefore the south boundary can be determined.

To simulate the flow field, CMS-Flow was driven by the measured tide at the offshore boundary. It is assumed that a 4-week record measured during July-August 2008 can adequately represent the offshore tidal variation. The 4-week record is therefore duplicated to cover a 2-year period (Figure 6). The WIS (Wave Information Study) hindcast data, developed by the U.S. Army Corps of Engineers (USACE), was used to provide a continuous wave record. The closest WIS station is located approximately 30 km offshore Johns Pass at 17-m water depth, or about 27 km seaward of the ocean boundary. Snell's Law and simple wave shoaling (assuming straight and parallel contour and neglecting friction) were applied to transform wave from the 17 m water depth to 7 m at the seaward boundary of the modeling domain. After examining a 20-year (1980-1999) WIS record, waves during two years, 1997 and 1999, were judged to be representative and used in the 2-year modeling effort (Figure 7). Wind forcing is inherently incorporated in the hindcast wave data and was, therefore, not considered separately. A spatially constant grain size of 0.26 mm, roughly representing the average size in the study area, was input to the CMS based on analysis of a large number of samples.

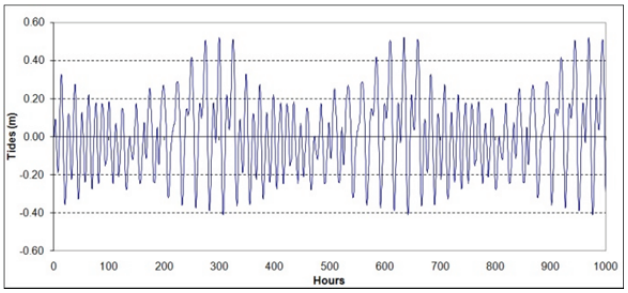

Figure 6. Input tides at the ocean boundary. A section of 1,000 hours over a 2-year period is shown here.

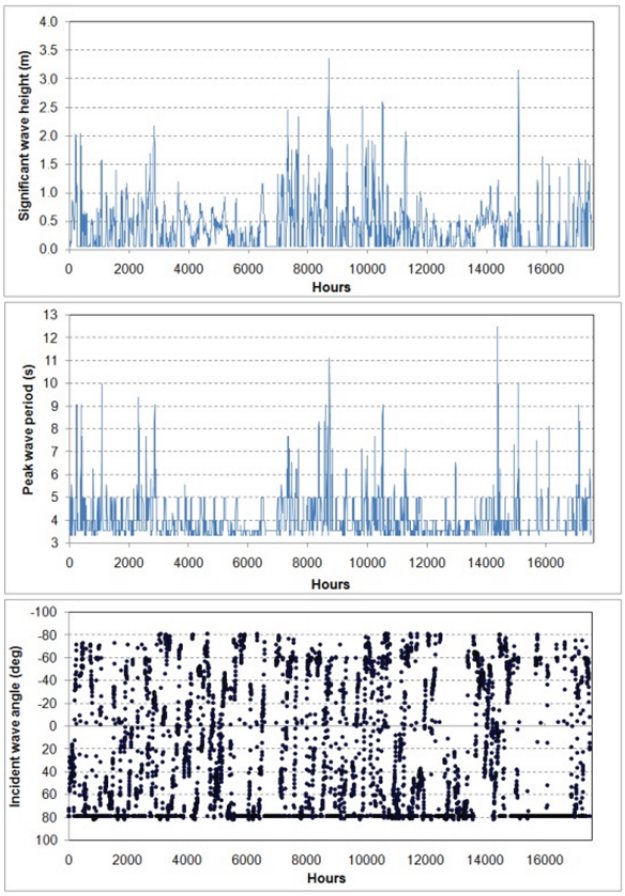

Figure 7. The input incident wave conditions. Upper: significant wave heights at the ocean boundary for the 2-year model run. A 5 cm wave height was arbitrarily assigned for waves that were propagating from land to sea, *e.g.*, driven by easterly wind. Middle: Peak wave period. Lower: incident wave angle, 0 = incident from west; -90 = incident from north; 90 = incident from south. A 78 deg angle was arbitrarily assigned for waves (5 cm high) that were propagating from land to sea

RESULTS AND DISCUSSION

The present study focuses on several challenging aspects of modeling a dual-inlet system. Its overall hydrodynamics, *e.g.*, tidal prism, are dominated by one inlet, Johns Pass. In terms of sediment transport, several mechanisms should be accurately captured, including forcing from the tide- and wave-induced current, waves (breaking and non-breaking), and combined wave and current. Executing model runs to simulate morphology change over 1 to 2 years is a challenge considering the needs of computation speed and stability.

Calculated Tidal Currents and Waves

Calculated water levels matched measurements well at both Johns Pass and Blind Pass (Figure 8). The calculated velocity at Johns Pass is considerably greater than those (measured and predicted) at Blind Pass (Figure 9), especially the ebb current velocity, indicating that CMS-flow captured the dominance of Johns Pass in this dual-inlet system. The faster tidal current

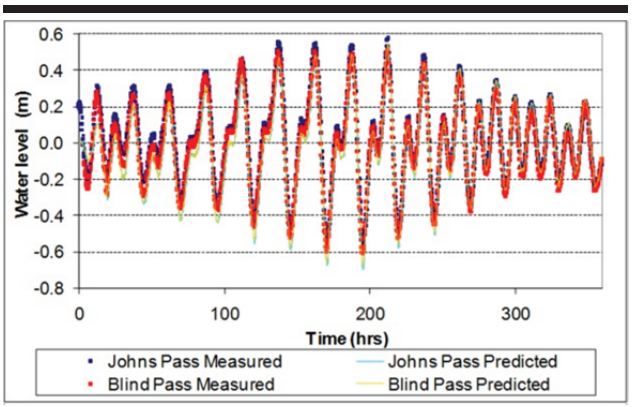

Figure 8. Measured and calculated water levels at Johns Pass and Blind Pass.

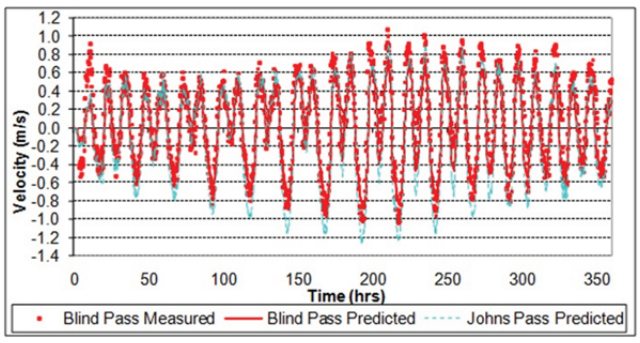

Figure 9. Measured and calculated current velocity at Blind Pass. Calculated velocity at Johns Pass is also illustrated.

through the much larger inlet cross-section yield a greater tidal prism at Johns Pass. Current meters were deployed at both inlets, but acoustic beams on the Johns Pass current meter malfunctioned. The calculated velocities at Blind Pass are as much as 25% lower than the measured velocities, especially during the peak of the ebb tide (Figure 9). Qualitative comparison of the calculated Johns Pass velocities with the measured values from previous deployments suggests that the predicted minimum and maximum velocities are similar. The default value of the bottom friction coefficient, a Manning's N value of 0.025 as recommended by CMS, is used here.

In addition to the current-velocity verification at one or several grid cells as discussed above, a qualitative approach was also used to examine computed regional patterns of the flow field, wave field, wave-current interaction, sediment transport, and morphology changes. Based on field observations, Wang *et al.* (2007) found that morphology changes are controlled by temporal and spatial variations (*i.e.*, gradients) of hydrodynamics and sediment transport. For example, the 90-deg turn of Blind Pass resulted in a strong ebb flow (~1 m/s) along the southeast side of the inlet and a weak ebb flow (~0.4 m/s) along the northwest side, whereas the flood flow is rather uniform across the entire inlet. This tidal flow pattern is responsible for the preferential sedimentation in the channel and is well-represented by the CMS. At Johns Pass, the strong ebb jet, extending to the seaward edge of the ebb-tidal delta is reproduced by the model.

Patterns of wave propagation and wave-current interaction are crucial to sediment transport and morphology change at Johns Pass and Blind Pass. Wang *et al.* (2007) found that the frequent passages of winter cold fronts and the associated northerly approaching high waves are the dominating mechanism driving morphology change. In the following, the calculated interactions of a northerly approaching high wave and peak flooding and ebbing currents at both Johns Pass and Blind Pass are discussed as a representative key example.

Under high northerly approaching waves, strong southward wave-driven current is predicated in the nearshore zone and over the Johns Pass ebb-tidal delta (Figures 10 and 11). Interaction of the longshore current and flood current leads to the formation of a large eddy downdrift of the inlet, resulting in a current reversal at the chronically eroding Sunshine Beach (Figure 10). Under a peak ebb flow, the southward longshore current along the updrift beach is blocked by the strong ebb jet, forming a large eddy north of the inlet (Figure 11). This particular flow pattern is responsible for the development of the channel margin linear bar and the associated mixed-energy morphology of the ebb-tidal delta. A strong southward longshore current was calculated along the terminal lobe under both flood and ebb conditions (Figures 10 and 11). This current converges with the nearshore longshore current primarily at the attachment point providing a pathway for southward sand bypassing.

The wave-current interaction during a passage of a modeled cold front at Blind Pass follows a different pattern from that observed at Johns Pass, and has been evolving since the last channel dredging in 2000 as modified by the developing morphology. Overall, the weak tidal flow is overwhelmed by the strong longshore current that flows across the inlet entrance under both flood (Figure 12) and ebb (Figure 13) conditions. A weak current was calculated along the northern portion of the entrance channel, which is consistent with field observations. A strong longshore current was calculated around the north jetty during flood tide, approaching 1 m/s (Figure 12) and is responsible for transporting sediment into the inlet. The relatively weak ebb flow is deflected by the stronger southward longshore current (Figure 13) resulting in a continuous flow along the downdrift Upham Beach. This circulation and sediment transport pattern corresponds with the strong erosive trend observed there, indicating that the CMS is capable of capturing this key mechanism inducing the observed rapid shoreline recession downdrift of Blind Pass (Elko *et al.*, 2005; Elko and Wang, 2007).

Calculated Sediment Transport

Sediment transport processes at tidal inlets are complex involving both current and wave forcing. Wave breaking occurs over a large portion of the ebb-tidal delta and along the adjacent shoreline, and breaking-induced sediment suspension and transport play crucial roles in inlet morphodynamcis and must be accurately represented. In the following, the same examples as used above in the discussion of wave-current interaction are presented to illustrate calculated sediment transport patterns during the passage of a cold front. The modeled transport used the empirical relationships (with default coefficients) defined in the Lund-CIRP formula (Larson and Camenen, this issue) for non-cohesive sediment transport. An adaptation length, or scaling of the transport capacity, (Sanchez and Wu, this issue) of 10 m was used for the NET computation of transport.

Comparing the calculated flow field (Figure 10) and sediment transport pattern (Figure 14) at Johns Pass under a flooding tide, the significance of breaking waves on sediment suspension and transport is clearly illustrated. The greatest depth-averaged sediment concentration and rate of sediment transport occur at locations with a combination of wave breaking (shallow water) and strong current. For this situation, greater sediment concentration and rates of sediment transport were predicted in three areas, including: (1) in the nearshore area north of the inlet, (2) over the channel margin linear bar, and (3) along the terminal lobe of the downdrift portion of the ebb-tidal delta. Channel infilling can result from the elevated transport in area 2. Although strong flow was predicted through the deep channel thalweg, relatively lower depth-averaged sediment concentrations and rates of transport were predicted. This wave-breaking induced sediment suspension and pattern of transport are captured by the CMS. A divergence of sediment transport was calculated at Sunshine Beach, directly south of Johns Pass and is responsible for the erosive trend observed there.

The sediment suspension and transport at Johns Pass under peak ebb current is different from that of the flood current (Figure 15). Greater depth-averaged sediment concentrations and rates of sediment transport were calculated in three areas: (1) in the nearshore area north of the inlet, (2) the channel margin linear bar and the nearby ebb channel, and (3) along the terminal and downdrift lobe of the ebb-tidal delta. The active sediment transport in area 1 under both flood and ebb tides is responsible for the development of the ebb-tidal delta. The active transport in are 2 represents sediment flushing by the

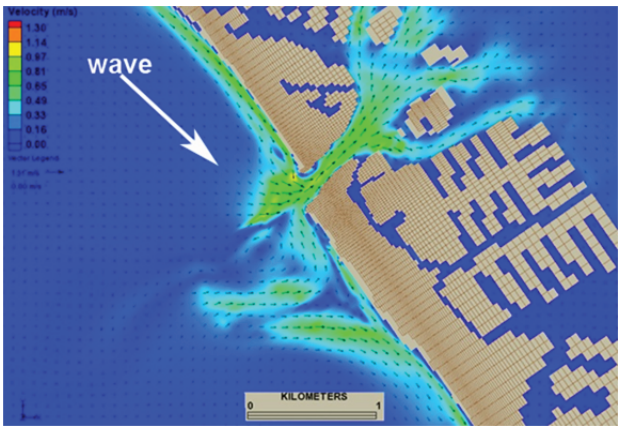

Figure 10. Calculated wave-current interaction at Johns Pass, under a high northerly approaching (arrow) wave with H_s=1.9 m and T_p=7.7 s, during a peak flooding tide.

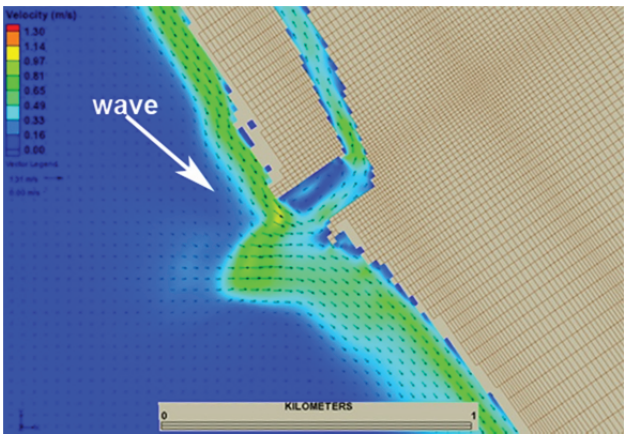

Figure 12. Calculated wave-current interaction at Blind Pass, under a high northerly approaching (arrow) wave with H_s=1.9 m and T_p=7.7 s, during a peak flooding tide.

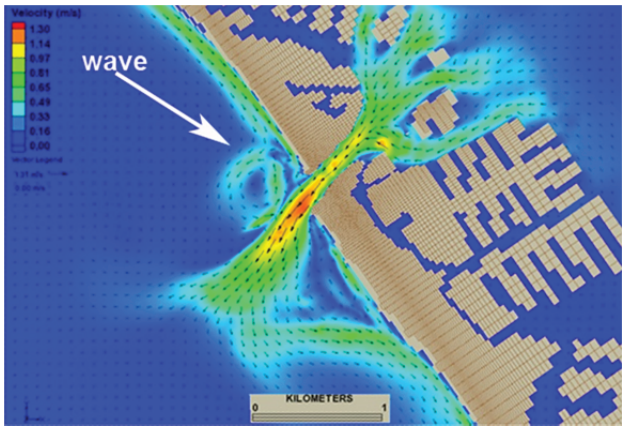

Figure 11. Calculated wave-current interaction at Johns Pass, under a high northerly approaching (arrow) wave with H_s=2.0 m and T_p=6.1 s, during a peak ebbing tide.

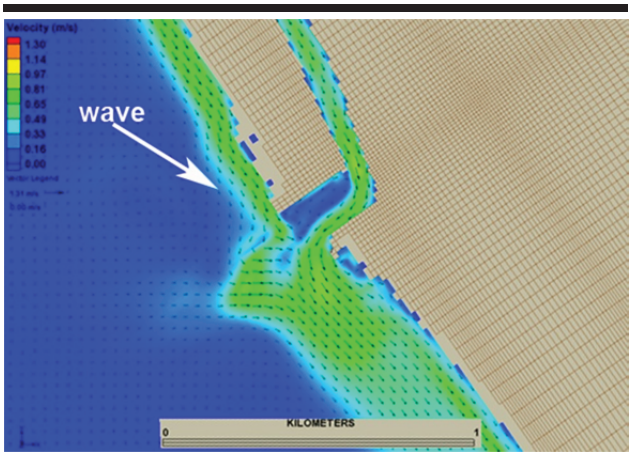

Figure 13. Calculated wave-current interaction at Blind Pass, under a high northerly approaching (arrow) wave with H_s=2.0 m and T_p=6.1 s, during a peak ebbing tide.

ebb jet. The strongest flow through the channel thalweg does not correlate with the greatest sediment concentration due to the lack of wave-breaking induced active sediment suspension. Similar to the flood tide case, the active sediment transport in area 3 provides the mechanism for sand bypassing across the inlet.

At Blind Pass, under peak flood flow (Figure 16), greater depth-averaged sediment concentrations and transport rates were calculated in three areas: (1) along the Sunset Beach north of the inlet, (2) over the newly developed ebb-tidal delta, and (3) along the downdrift Upham Beach. Active sediment transport in areas 1 and 2 contributes to sedimentation in the inlet channel. The erosion along the updrift Sunset Beach and downdrift Upham Beach corresponds to the active transport in areas 1 and 3.

Figure 17 illustrates the calculated sediment transport pattern during a peak ebb tide. Elevated sediment concentrations and transport rates were predicted in two areas, the updrift Sunset Beach and extending into the inlet, and across the main ebb channel and along the downdrift Upham Beach. The weak ebb current along the northern side of the inlet is not capable of flushing the sediment deposited during the flood tide. The southward deflected ebb jet and strong longshore current resulted in intensified southward longshore transport along Upham Beach. This pattern is also interpreted from field observations (Wang *et al.*, 2007) suggesting that the model correctly captured sediment transport at Blind Pass. Overall, the

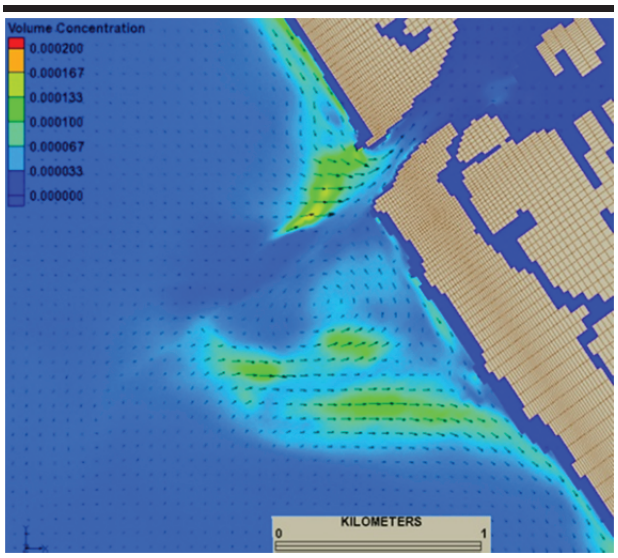

Figure 14. Calculated depth-averaged sediment volume concentration (dimensionless) and transport vectors at Johns Pass, under a high northerly approaching wave with H_s=1.9 m and T_p=7.7 s, during a peak flooding tide.

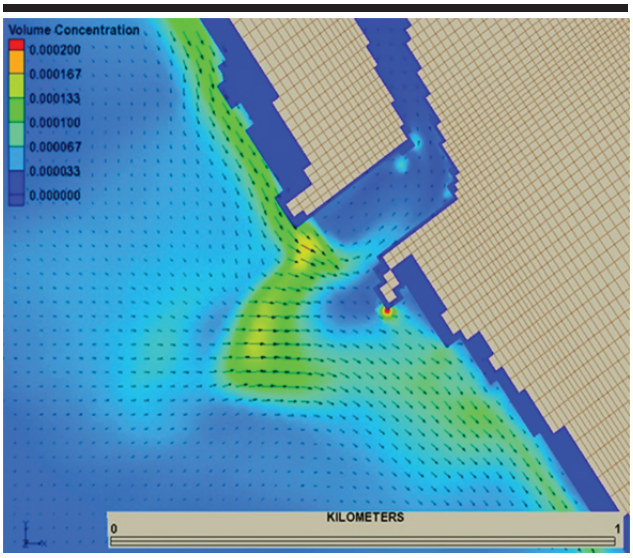

Figure 16. Calculated depth-averaged sediment volume concentration (dimensionless) and transport vectors at Blind Pass, under a high northerly approaching wave with H_s=1.9 m and T_p=7.7 s, during a peak flooding tide.

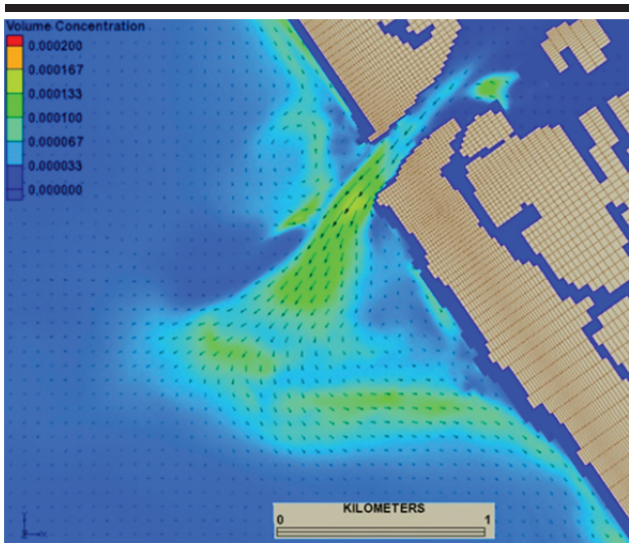

Figure 15. Calculated depth-averaged sediment volume concentration (dimensionless) and transport vectors at Johns Pass, under a high northerly approaching wave with H_s=2.0 m and T_p=6.1 s, during a peak ebbing tide.

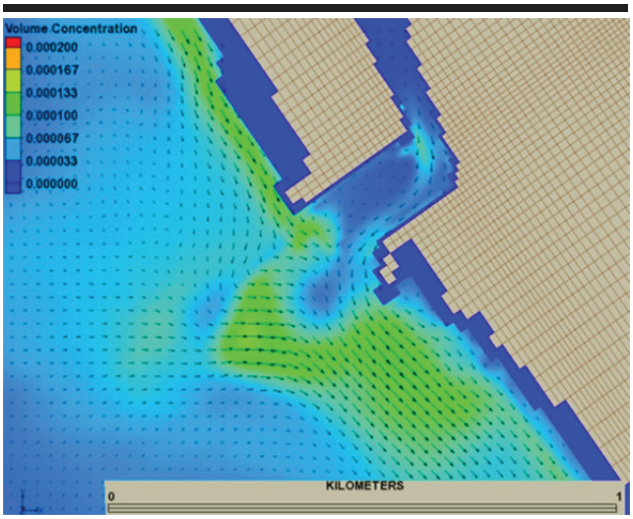

Figure 17. Calculated depth-averaged sediment volume concentration (dimensionless) and transport vectors at Blind Pass, under a high northerly approaching wave with H_s=2.0 m and T_p=6.1 s, during a peak ebbing tide.

calculated sediment transport patterns agree with several key observed morphology trends at the dual-inlet system.

Calculated Medium-term Morphology Change

The following discussion examines the capability of the CMS to predict key trends of morphology change, *e.g.*, accumulation

of sediment at the updrift beach, downdrift beach erosion, and sediment bypassing over the ebb-tidal delta. For the case of Johns Pass and Blind Pass, the sediment traps created by dredging provide an opportunity to verify the capability of CMS to predict sedimentation in dredged pits, for which the sedimentation rate is closely related to the gross and net longshore transport rate. In addition, dredged pits tend to experience rapid morphology change and provide ideal sites for verification of medium-term morphology modeling. The dredging of Blind Pass in the summer of 2000 (Figure 4) created a total trap for the southward longshore sediment transport. The rate and pattern of sedimentation in the dredged pit were quantified by Wang *et al.* (2007). Figure 18 shows the calculated bathymetry in comparison with the measurements.

Sedimentation measured in the northern portion of the inlet, particularly along the north jetty and around the 90-deg turn, was captured by the CMS. The calculated sedimentation was episodic, driven by high-wave events associated with cold front passages, and agrees well with field measurements. This indicates that CMS reproduced, at least qualitatively, the temporal variations of sediment transport and morphology change. The calculated sedimentation rate is 32,000 m^3/year in the Blind Pass dredged pit, comparing well with the measured value of 35,000 m^3/year. Erosional trends along the updrift Sunset Beach and downdrift Upham Beach were also modeled by CMS. An accretionary trend, benefiting from the sand supply from Upham Beach, was predicted downdrift of the erosional hotspot. The considerable bathymetry smoothing, or erosion of the local positive morphology features (*e.g.*, the developing ebb delta), is not realistic based on the morphology trends observed over the last nine years.

At Johns Pass, a dredged pit along the updrift side of the main channel was designed in the model grid after the typical maintenance dredging configuration (Figure 19). CMS predicted a sedimentation rate in the dredged pit of 60,000 m^3/year, which agrees with the commonly accepted gross longshore transport rate estimated by Walton (1973). Accretionary trends predicted at the attachment point and along the south jetty agree with field observations. The erosive trend along the southern side of the channel (location of the thalweg) and accretionary trend along the northern portion also agree with field observations. However, because a constant grain size of 0.26 mm was specified, the coarse channel lag was not accounted for, and excessive channel scour was predicted.

Overall, CMS reproduced several key trends of sediment transport and morphology change including downdrift beach erosion, transport reversals induced by wave refraction, sediment bypassing around the ebb-tidal delta, and accretion at the attachment point. The magnitude of calculated sedimentation rates compare well with the field measurements. The model runs did not apply any schematization, *i.e.*, no morphology acceleration factors were applied. The 1.2- to 1.6-year simulated period was computed using mostly default values suggested by CMS.

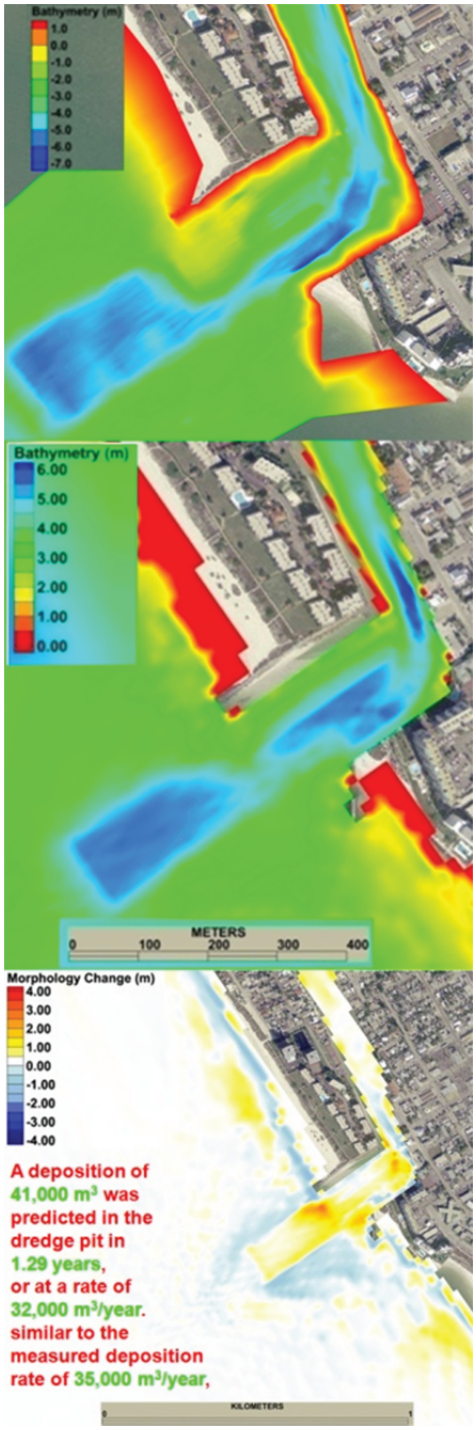

Figure 18. Measured and Calculated bathymetry at Blind Pass. Top: Measured bathymetry 1 year after dredging (Figure 4 shows the post-dredging bathymetry); Middle: Calculated bathymetry 1.29 years after dredging; Lower: Calculated bathymetry change; red colors = accretion; blue colors = erosion.

SUMMARY AND CONCLUSIONS

The Coastal Modeling System (CMS) successfully combined numerical computation of tidal current, wave, sediment transport

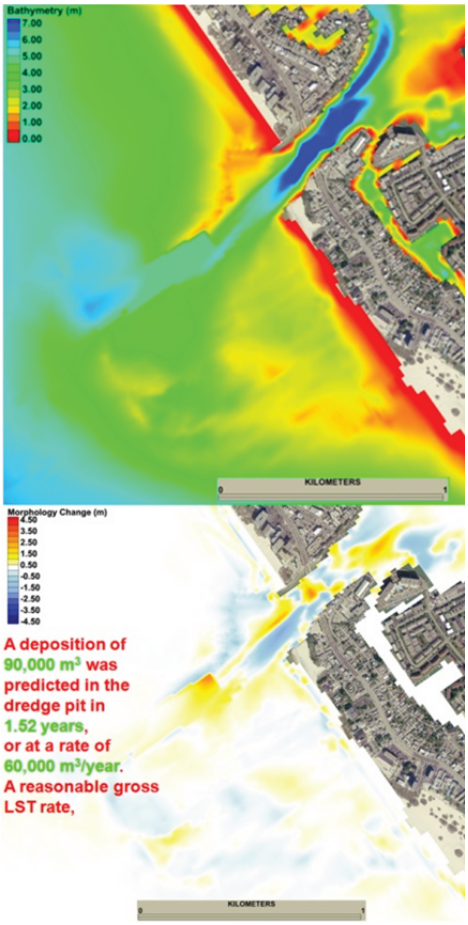

Figure 19. Calculated bathymetry at Johns Pass. Upper: initial bathymetry with a designed dredged pit; Lower: calculated bathymetry changes 1.52 years after; red colors = accretion; blue colors = erosion.

and morphology change. The CMS realistically reproduced the observed medium-term morphology change at the interactive Johns Pass and Blind Pass, a dual-inlet system, in West-Central Florida. The calculated hydrodynamics, sediment transport, and morphology change were compared with extensive field data. Observed stronger tidal-driven flow through the dominating Johns Pass, and weaker flow through the secondary Blind Pass, was calculated indicating that the CMS captured the key hydrodynamic patterns of this interactive dual-inlet system. The complicated wave refraction and breaking over the ebb-tidal delta was simulated and comparable to field observations, leading to a realistic representation of the wave-current interaction. Wave-breaking induced elevated sediment suspension and transport were captured by CMS.

The calculated morphology change from 1.2- to 1.6-year model simulations compared well with field measurements. Several key spatial trends of morphology change, *e.g.*, erosion along the downdrift beach, accretion at the attachment point, and sedimentation in the channel were reproduced by the model. The calculated morphology change illustrated heightened responses to high-energy wave events, consistent with field observations of episodic evolution of the inlets and adjacent bathymetry. Artificially dredged pits provide sediment traps for comparison and verification of the overall computed sedimentation rates. A sedimentation rate of 32,000 m^3/year calculated by CMS agrees well with the measured rate of 35,000 m^3/year at the Blind Pass dredged pit and the net rate of southward longshore transport. The calculated sedimentation rate of 60,000 m^3/year for the designed dredge pit at Johns Pass agrees with the generally accepted gross rate of longshore transport.

ACKNOWLEDGMENTS

This study was supported by US Army Engineer Research and Development Center's (ERDC) Coastal Inlet Research Program (CIRP), Pinellas County Florida, and the University of South Florida. Permission was granted by Headquarters, U.S. Army Corps of Engineers, to publish this information.

REFERENCES

Aubrey, D.G. and Giese, G.S., 1993. *Formation and evolution of multiple tidal inlets*. American Geophysical Union-Coastal and Estuarine Studies, No. 44, 237p.

Barnard, P.L., 1998. Historical Morphodynamics of Inlet Channels: West-Central Florida. *MS thesis*, Tampa, Florida: Department of Geology, University of South Florida, 179pp.

Bruun P., 1978. *Stability of Tidal Inlet: Theory and Engineering*. Elsevier Scientific Publishing Company, Amsterdam, 510 pp.

Buttolph A.M.; Reed, C.W.; Kraus, N.C.; Ono, N.; Larson, M.; Camenen, B.; Hanson, H.; Wamsley, T., and Zundel, A.K., 2006. Two-dimensional depth-averaged circulation model CMS-M2D: Version 3.0, Report 2, sediment transport and morphology change, *ERDC/CHL TR-06-9*, Vicksburg, Mississippi: U.S. Army Engineer Research and Development Center, 149pp.

Camenen, B. and Larson, M., 2007. A Unified Sediment Transport Formulation for Coastal Inlet Application. *ERDC/CHL CR-07-1*, Vicksburg, Mississippi: U.S. Army Engineer Research and Development Center, 231 pp.

CPE (Coastal Planning & Engineering, Inc.), 1992. *Blind Pass Inlet Management Plan*. Pinellas County, Florida: 68pp.

CPE (Coastal Planning & Engineering, Inc.), 1993. *Johns Pass Inlet Management Plan*. Pinellas County, Florida: 31pp.

Dean, R.G., 1988. Sediment interaction at modified coastal inlets: Processes and policies. *Lecture Notes on Coastal and Estuarine Studies*, Vol. 29, 412-439.

Elko, N.A.; Holman, R.A.; Gelfenbaum, G., 2005. Quantifying the rapid evolution of a nourishment project with video imagery. *Journal of Coastal Research*, 21 (4), 633–645.

Elko, N.A. and Wang, P., 2007. Immediate profile and planform evolution of a beach nourishment project with hurricane influences. *Coastal Engineering*, 54, 54-79.

Fitzgerald, D.M., 1996. Geomorphic variability and morphologic and sedimentologic controls on tidal inlets. *Journal of Coastal Research*, 23, 47–71.

Kraus, N.C., 2009. Engineering of tidal inlets and morphologic consequences. In Y.C. Kim (ed.), *Handbook of Coastal and Ocean Engineering*, World Scientific, 867-901.

Kraus, N.C. and Militello, A., 1999. Hydraulic study of multiple inlet system: East Matagorda Bay, Texas. *Journal of Hydraulic Research*, 125(3), 224-232.

Larson L. and Camenen, B., this issue. A unified sediment transport model for inlet application. *In:* Roberts, T.M., Rosati, J.D., and Wang, P. (eds.), *Proceedings, Symposium to Honor Dr. Nicholas C. Kraus,* Journal of Coastal Research, Special Issue, No. 59. West Palm Beach (Florida)

Lin, L., Demirbilek, Z., Mase, H., Zheng, J., and Yamada, F., 2008. CMS-Wave: A Nearshore Spectral Model for Coastal Inlets and Navigation Projects. *ERDC/CHL TR-08-13*, Vicksburg, Mississippi: U.S. Army Engineer Research and Development Center, 120pp.

Lin, L.; Mase, H.; Yamada, F., and Demirbilek, Z., 2006. Wave Action Balance Equation Diffraction (WABED) Model: Tests of Wave Diffraction and Refraction at inlets. *ERDC/CHL CHETN-III-3*, Vicksburg, Mississippi: U.S. Army Engineer Research and Development Center, 24pp.

Lin L.; Kraus N.C., and Demirbilek, Z., this issue. CMS-Wave: A coastal wave model for inlets and navigation projects. *In:* Roberts, T.M., Rosati, J.D., and Wang, P. (eds.), *Proceedings, Symposium to Honor Dr. Nicholas C. Kraus,* Journal of Coastal Research, Special Issue, No. 59. West Palm Beach (Florida)

Mase, H. and Kitano, T., 2000. Spectrum-based prediction model for random wave transformation over arbitrary bottom topography. *Coastal Engineering Journal* (JSCE), 42, 111-151.

Mase, H., 2001. Multidirectional random wave transformation model based on energy balance equation. *Coastal Engineering Journal* (JSCE), 43, 317-337.

Mase, H.; Oki, K.; Hedges, T.S., and Li, H., 2005. Extended energy-balance-equation wave model for multidirectional random wave transformation. *Ocean Engineering*, 32, 961-985.

Mehta, A.J.; Adams, W.D., and Jones, C.P., 1976. Johns Pass and Blind Pass: Glossary of Inlets Report Number 4. Florida Sea Grant Program, *Report Number 18*, 66pp.

Reed, C.; Brown, M.; Lin, L., and Kraus, N.C., this volume. CMS-Flow: a coastal tidal model for inlets and navigation projects. *In:* Roberts, T.M., Rosati, J.D., and Wang, P. (eds.), *Proceedings, Symposium to Honor Dr. Nicholas C. Kraus,* Journal of Coastal Research, Special Issue, No. 59. West Palm Beach (Florida)

Sanchez, A. and Wu, W., this volume. Application of a coupled current, wave and non-equilibrium sediment transport model for coastal inlets. *In:* Roberts, T.M., Rosati, J.D., and Wang, P. (eds.), *Proceedings, Symposium to Honor Dr. Nicholas C. Kraus,* Journal of Coastal Research, Special Issue, No. 59. West Palm Beach (Florida)

Tanner, W.F., 1960. Florida coastal classification. *Transactions – Gulf Coast Association of Geological Science*, Volume 10, 259-266.

van de Kreeke, J., 1990. Can multiple inlets be stable? *Estuarine Coastal and Shelf Science*, 30, 261-273.

van de Kreeke, J; Brouwer, R. L.; Zitman, T. J., and Schuttelaars, H. M., 2008. The effect of a topographic high on the morphological stability of a two-inlet bay system. *Coastal Engineering*, 55, 319-332.

Walton, T.L., Jr., 1973. Littoral Drift Computations along the Coast of Florida by Means of Ship Wave Observations. *Coastal and Oceanographic Engineering Laboratory Technical Report No. 15*, University of Florida, Gainesville, Florida, 80p.

Wang, P. and Davis, R.A., 1999. Depth of closure and the equilibrium beach profile – A case study from Sand Key, West-Central Florida. *Shore and Beach*, 67, 33-42.

Wang, P.; Tidwell, D.K.; Beck, T.M., and Kraus, N.C., 2007. Sedimentation patterns in a stabilized migratory inlet, Blind Pass, Florida, *Proceedings of Coastal Sediments 07*. ASCE Press, 1377-1390.

Wang, P.; Roberts, T.M.; Elko, N.A., and Beck, T.M., 2008. Factors controlling the first year performance of eight adjacent beach nourishment projects, west-central Florida, USA, *Proceedings of the 31st International Conference on Coastal Engineering*. World Scientific, 2532-2544.

Wu, W., 2008. *Computation River Dynamics*. Taylor and Francis, London, 589pp.